Overview of Polarimetric Interferometry

Yunjin Kim and Jakob van Zyl
Jet Propulsion Laboratory
California Institute of Technology
4800 Oak Grove Drive
Pasadena, CA 91109-8099

Tel: (818) 354-9500
Fax: (818) 393-5285
E-mail: ykim@radar-sci.jpl.nasa.gov

Abstract— SAR (Synthetic Aperture Radar) interferometry has enabled two important science applications: surface change detection and topographic mapping. SAR interferometry is sensitive to the location of the imaged area and the scattering geometry. SAR polarimetry makes use of the polarization dependent scattering response of each pixel within the imaged area. The polarimetric response is highly sensitive to the scattering mechanism of a pixel. S. R. Cloude and K. P. Papathanassiou first published the formulation of polarimetric interferometry that combines both SAR interferometry and SAR polarimetry. The main purpose of using polarimetric interferometry is to extract scattering medium information that may be difficult to obtain from scalar interferometry. Even though the formulation and initial demonstrations appear to be very promising, potential applications of polarimetric interferometry can only be verified by comparing polarimetric interferometry signatures with ground truth data. In this talk, we present the theory and implementation of SAR polarimetric interferometry. Especially, we review SAR polarimetry, SAR interferometry, and SAR polarimetric interferometry in a unified manner. In addition, a new calibration technique suitable for polarimetric interferometry is suggested in this paper.

TABLE OF CONTENTS

1. INTRODUCTION

Natural objects scatter an electromagnetic wave differently depending upon the incident wave polarization. In 1852, Stokes described partially polarized light by using the Stokes parameters. In 1946, George Sinclair used a 2 x 2 coherent scattering matrix to illustrate the radar target property as a polarization transformer. In the 1960s and 1970s, many researchers studied various remote sensing applications based on radar polarimetry [1]. The NASA/JPL AIRSAR system is considered to be the first imaging radar polarimeter [2]. By using imaging radar, the polarimetric characteristic can be measured for each pixel to understand the scattering mechanism associated with it. Even though the physical property of a pixel may not be easily recognized by the polarimetric response, the geophysical information associated with the scattering mechanism may be inferred from the polarimetric response.

SAR interferometry has enabled two important science applications: surface change detection and topographic mapping [1]. Interferometric measurements are obtained from subtle phase signatures shown in two SAR images; therefore, the two images must be coherent. The correlation between two SAR images depends on various parameters: SNR (Signal to Noise Ratio), the pixel scattering property, the radar imaging geometry, and the temporal change of the imaged area. The temporal decorrelation becomes significant if two images are not obtained simultaneously. In 1974, Graham reported the first airborne interferometric SAR system that generated topographic contours using the hardware interference system [3]. The NASA/JPL AIRSAR system demonstrated the DEM (Digital Elevation Model) production capability in 1986. This across track interferometric mode is popularly known as TOPSAR. The interferometric correlation coefficient depends on the scattering mechanism. Even though the correlation coefficient does not uniquely depend on the scattering geometry, an empirical approach may be developed to produce useful physical information from the interferometric correlation.

S. R. Cloude and K. P. Papathanassiou first published the formulation of polarimetric interferometry that combines both SAR interferometry and SAR polarimetry [4]. That is, the interferometric response of each pixel is measured for various polarization combinations. In this way, the optimum polarization for SAR interferometry can be selected to improve the interferometric SAR image quality. Since the polarimetric response is sensitive to the scattering mechanism, detailed scattering characteristics can be estimated by using polarimetric interferometry.

0-7803-5846-5/00/$10.00 © 2000 IEEE

2. SAR POLARIMETRY

In this section, we discuss various coherent scattering vectors to represent polarimetric SAR data. The polarimetric SAR implementation is shown in Fig. 1. The polarimetric data collection is performed in two sequences as denoted by (1) and (2). In this way, all four elements in the scattering matrix can be measured.

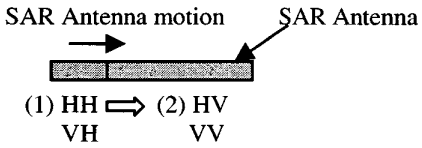

Fig. 1. Polarimetric SAR implementation. A radar polarimeter involves transmitting a wave of one polarization and receiving echoes in two orthogonal polarizations simultaneously (sequence 1). This is followed by transmitting a wave with a second polarization, and again receiving echoes with both polarizations simultaneously (sequence 2).

It has been shown that the polarization decomposition can provide useful geophysical information. Using the linear polarization basis, the scattering vector $\bar{k}_L$ can be written as

$$\bar{k}_L = \begin{bmatrix} S_{hh} \\ \sqrt{2}S_{hv} \\ S_{vv} \end{bmatrix} \tag{1}$$

where S_{xy} means the scattering response when a transmit electromagnetic wave is y-polarized while the receive antenna is x-polarized. Another coherent scattering vector using the Pauli matrix basis is given by

$$\bar{k}_P = \frac{1}{\sqrt{2}} \begin{bmatrix} S_{hh} + S_{vv} \\ 2S_{hv} \\ S_{vv} - S_{hh} \end{bmatrix} \tag{2}$$

The coherent scattering vector using the circular polarization basis can be expressed as

$$\bar{k}_C = \frac{1}{2} \begin{bmatrix} S_{hh} - S_{vv} + 2iS_{hv} \\ S_{hh} + S_{vv} \\ S_{hh} - S_{vv} - 2iS_{hv} \end{bmatrix} \tag{3}$$

When $\bar{k}_L$ and $\bar{k}_P$ are compared, the power associated with each element provide different information. That is,

$$P_L = \left\langle \bar{k}_L . \bar{k}_L^{+} \right\rangle = \begin{bmatrix} \left\langle S_{hh} S_{hh}^{*} \right\rangle \\ 2\left\langle S_{hv} S_{hv}^{*} \right\rangle \\ \left\langle S_{vv} S_{vv}^{*} \right\rangle \end{bmatrix} \tag{4}$$

However, the coherent scattering vector using the Pauli matrix basis includes the co-polarized phase difference as shown in equation (5).

$$P_P = \left\langle \bar{k}_P . \bar{k}_P^{+} \right\rangle = \frac{1}{2} \begin{bmatrix} \left\langle S_{hh} S_{hh}^{*} \right\rangle + \left\langle S_{vv} S_{vv}^{*} \right\rangle + 2\left\langle |S_{hh}||S_{vv}| \cos(\phi_{hh} - \phi_{vv}) \right\rangle \\ 4\left\langle S_{hv} S_{hv}^{*} \right\rangle \\ \left\langle S_{hh} S_{hh}^{*} \right\rangle + \left\langle S_{vv} S_{vv}^{*} \right\rangle - 2\left\langle |S_{hh}||S_{vv}| \cos(\phi_{hh} - \phi_{vv}) \right\rangle \end{bmatrix} \tag{5}$$

Notice that the total power is conserved regardless of the polarization representation.

To understand polarimetric parameters that may contain the geophysical information, we also examined the correlation coefficients that can be obtained as

$$[T] = \bar{k} \cdot \bar{k}^{+} \tag{6}$$

where + denotes the transpose and complex conjugate operation. Nine independent quantities can be obtained from equation (6): three backscattering cross sections and three complex (amplitude and phase) cross correlation coefficients. This cross correlation combination can be accomplished by using various coherent scattering vectors such as one using the Pauli matrix basis. The usefulness of these correlation coefficients can only be evaluated when they are compared with ground truth data.

The average covariance matrix $[T]$ [5] for azimuthally symmetric scattering objects can be written as

$$[T] = C \begin{bmatrix} 1 & 0 & \rho \\ 0 & \eta & 0 \\ \rho^{*} & 0 & \zeta \end{bmatrix} \tag{7}$$

where

$$C = \left\langle S_{hh} S_{hh}^{*} \right\rangle \tag{8}$$

$$\rho = \frac{\left\langle S_{hh} S_{vv}^{*} \right\rangle}{C} \tag{9}$$

$$\eta = 2\frac{\langle S_{hv} S_{hv}^* \rangle}{C} \tag{10}$$

$$\zeta = \frac{\langle S_{vv} S_{vv}^* \rangle}{C} \tag{11}$$

The *hh-vv* cross correlation (ρ) is particularly useful for estimating biomass. Then, the covariance matrix can be decomposed into eigenvalues (λ) and eigenvectors (κ) as

$$[T] = \lambda_1 \kappa_1 \cdot \kappa_1^+ + \lambda_2 \kappa_2 \cdot \kappa_2^+ + \lambda_3 \kappa_3 \cdot \kappa_3^+ \tag{12}$$

The strength of eigenvalues can be used for identifying the scattering mechanism associated with each pixel.

The coherent scattering vector can be written in various ways. Another representation of the polarimetric response can be accomplished by writing the coherent scattering vector as

$$\vec{k} = |\vec{k}|\hat{u} \tag{13}$$

where $|\vec{k}|^2$ is proportional to the scattering power and the unitary complex vector $\hat{u}$ is written as

$$\hat{u} = \begin{bmatrix} \cos\alpha \; e^{i\phi_1} \\ \sin\alpha\cos\beta \; e^{i\phi_2} \\ \sin\alpha\sin\beta \; e^{i\phi_3} \end{bmatrix} \tag{14}$$

Then, $|k|^2$, α, β, $\phi_1 - \phi_2$, and $\phi_2 - \phi_3$ can be used to characterize the polarimetric scattering response.

3. SAR INTERFEROMETRY

SAR interferometry uses two data sets (S_u and S_l) obtained from both upper and lower antennas. Interferometric data products can be summarized by using equation (15) as

$$\begin{bmatrix} S_u \\ S_l \end{bmatrix} \begin{bmatrix} S_u^* & S_l^* \end{bmatrix} = \begin{bmatrix} S_u S_u^* & S_u S_l^* \\ S_l S_u^* & S_l S_l^* \end{bmatrix} \tag{15}$$

The diagonal terms are usual SAR images and the off-diagonal terms provide the interferometric information. The implementation of SAR interferometry is shown in Fig. 2.

The interferometric data collection can be accomplished in two ways. For the single baseline mode, the interferometric pair is measured simultaneously. The double baseline mode is implemented in two sequences as denoted by (1) and (2).

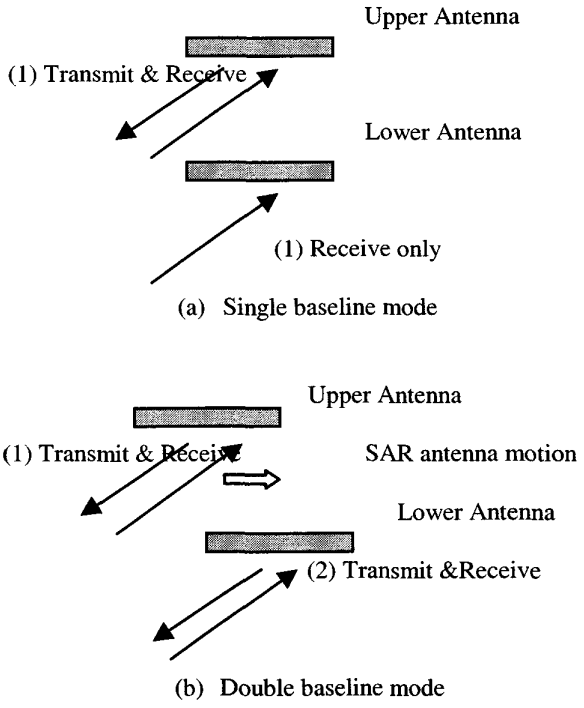

Fig. 2. SAR interferometry implementations. (a) The upper antenna transmits and both antennas receive a return echo simultaneously (sequence 1). (b) Both upper and lower antennas transmit and receive (sequence 1 and 2) . In this way, the effective baseline length is doubled.

The interferometric correlation coefficient can be expressed as

$$\gamma = \frac{\langle S_u S_l^* \rangle}{\sqrt{\langle S_u S_u^* \rangle \langle S_l S_l^* \rangle}} = \gamma_s \gamma_n \gamma_t \tag{16}$$

where $(1-\gamma_s)$, $(1-\gamma_n)$ and $(1-\gamma_t)$ represent scattering, thermal noise, and temporal decorrelation, respectively. The temporal decorrelation disappears if a single pass interferometry system is implemented. The phase of the correlation coefficient is used for generating DEM with proper phase unwrapping while its amplitude is related to the scattering mechanism.

Once the interferometric system is calibrated, the noise related decorrelation amount can be estimated. Therefore, we can isolate the scattering related decorrelation that is sensitive to the scattering geometry. From this scattering related decorrelation, one can estimate the tree height based

on a simple scattering model. For this application, the system must be well calibrated since the decorrelation value is very small. It is also advantageous to use multiple baselines if the multiple baseline configuration is available. This approach was successfully implemented by several researchers [6,7].

4. SAR POLARIMETRIC INTERFEROMETRY

Polarimetric interferometry combines both SAR polarimetry and SAR interferometry. The polarimetric interferometry system can be implemented by collecting polarimetric data for both upper and lower antennas as shown in Fig. 3. That is, the data collection is performed in four sequences as denoted by (1), (2), (3), and (4).

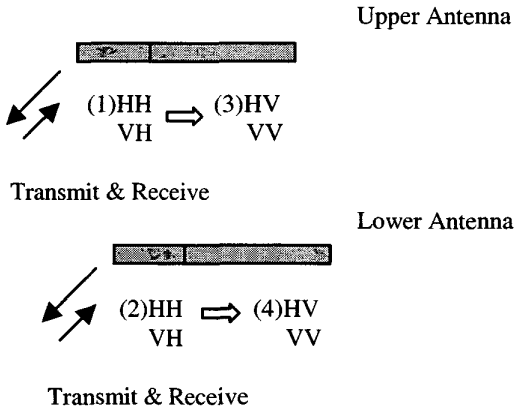

Fig. 3. SAR polarimetric interferometry implementation. Notice that this mode is a hybrid of SAR polarimetry and double baseline SAR interferometry. The upper antenna collects HH and VH (sequence 1) and the lower antenna collects HH and VH (sequence 2). This process repeats for the vertical polarization transmit case (sequences 3 and 4).

The polarimetric interferometry implementation as shown in Fig. 3 can be done in two ways: single pass and repeat pass data collections. Repeat-pass space-borne polarimetric interferometry data were obtained at two SIR-C frequencies (L- and C-band), with across-track interferometric baseline separations of 10 to 4700 m in 1994. These data sets suffer temporal decorrelation since we did not collect two polarimetric data simultaneously. In order to remove temporal decorrelation, the NASA/JPL AIRSAR system was modified to collect single pass polarimetric interferometry data at C-band [8]. Experimental polarimetric interferometry data were collected by the NASA/JPL AIRSAR system in 1998 and 1999 and these data sets are currently under calibration.

As noticed from Fig. 3, the polarimetric interferometry pulse repetition frequency (PRF) is twice as high as the PRF of the usual polarimetric SAR. Therefore, the data-limited swath is only half of the usual swath. In addition, since the cross polarization component has to be measured, the higher SNR (Signal to Noise Ratio) will be very useful for the polarimetric interferometry operation.

Using the linear polarization basis, output data products of SAR polarimetric interferometry can be written as

$$[T_{PI}] = \begin{bmatrix} \vec{k}_L^{(u)} \\ \vec{k}_L^{(l)} \end{bmatrix} \left[\vec{k}_L^{(u)*} \quad \vec{k}_L^{(l)*} \right] \tag{17}$$

where $[T_{PI}]$ is the polarimetric interferometry correlation matrix. In addition to the linear polarization basis, various coherent scattering vector representations can also be used to obtain cross correlation coefficients that enhance the geophysical features. Among the matrix elements in (17), two polarimetric data sets are collected for both upper and lower antennas. The differences in both polarimetric responses are expected to be minor. The same polarization interferometry data (such as $S_{hh}^{(u)} S_{hh}^{(l)*}$) can be used to derive DEMs and the decorrelation amount associated with each polarization. The hybrid polarization interferometry data (such as $S_{hh}^{(u)} S_{vv}^{(l)*}$) contains both polarization and interferometry dependent decorrelation. It is expected that each pixel can be characterized better by using both SAR polarimetry and SAR interferometry. The phase center and the correlation coefficient of each polarization response may be used to retrieve physical scattering features such as tree heights. The usefulness of these data sets must be evaluated by comparing them with the ground truth data. In order to do this evaluation, the polarimetric interferometry data must be calibrated carefully.

We propose the polarimetric interferometry calibration in two steps: the relative calibration between different polarization pairs and the usual interferometric calibration. Since the polarimetric interferometry signature can be relatively minute, it is necessary to perform the relative calibration precisely. That is, the calibration accuracy must be increased since the interferometric phase and correlation coefficient may not vary significantly for various polarization combinations. Then, the usual interferometric calibration can be applied to one polarization data and subsequently all polarization combinations will be calibrated.

Eight radar measurements are involved in the polarimetric interferometry calibration as shown in equation (18).

$$S_{hh}^{(u)}, S_{hv}^{(u)}, S_{vh}^{(u)}, S_{vv}^{(u)}, S_{hh}^{(l)}, S_{hv}^{(l)}, S_{vh}^{(l)}, S_{vv}^{(l)} \tag{18}$$

where the superscripts u and l denote the upper and the lower antennas, respectively. For the backscattering image, $S_{hv} = S_{vh}$; therefore, three homogeneous polarization interferograms

$(S_{hh}^{(u)}S_{hh}^{(l)*},\ S_{vv}^{(u)}S_{vv}^{(l)*},\ S_{vh}^{(u)}S_{vh}^{(l)*})$ are used derived for interferometric calibration: ϕ_{hh},ϕ_{vv} and ϕ_{hv}. The differential interferogram has all necessary information for relative polarization calibration. Mathematically

$$\begin{aligned}\Delta_{hhvv}(r,a) &= \phi_{hh}(r,a)-\phi_{vv}(r,a)\\ &= C_{hhvv}+B_{hhvv}(r,a)+Q_{hhvv}(r,a)\\ &+M_{hhvv}(r,a)+n_{hhvv}(r,a)\end{aligned} \tag{19}$$

$$\begin{aligned}\Delta_{hhhv}(r,a) &= \phi_{hh}(r,a)-\phi_{hv}(r,a)\\ &= C_{hhhv}+B_{hhhv}(r,a)+Q_{hhhv}(r,a)\\ &+M_{hhhv}(r,a)+n_{hhhv}(r,a)\end{aligned} \tag{20}$$

$$\begin{aligned}\Delta_{hvvv}(r,a) &= \phi_{hv}(r,a)-\phi_{vv}(r,a)\\ &= C_{hvvv}+B_{hvvv}(r,a)+Q_{hvvv}(r,a)\\ &+M_{hvvv}(r,a)+n_{hvvv}(r,a)\end{aligned} \tag{21}$$

where C is the constant phase (radar channel differential phase), B is the phase due to baseline vector difference, Q is the phase due to the different scattering mechanism, M is the multi-path phase, and n represents the thermal noise component. Here, (r,a) denotes the pixel location in the range (r) and azimuth (a) domain. If we average Δ in the along track direction of a homogeneous scene, the scattering related phase difference Q and the radar noise term n will be significantly reduced. That is, $\langle Q\rangle_a \approx \langle n\rangle_a \approx 0$. This technique is only effective when the aircraft motion is included. The average process should be based on the incidence angle to the aircraft since the multi-path effect depends on the aircraft geometry. After the average, the systematic phase error (Φ_s) can be obtained as

$$\Phi_s = \langle \Delta(\theta_{ac})\rangle = C + B(\theta_{ac}) + M(\theta_{ac}) \tag{22}$$

where θ_{ac} is the aircraft incidence angle. From Φ_s, one may be able to estimate the baseline error to derive the accurate baseline information. Since polarimetric interferometry implements the double baseline interferometry mode, the phase B can be expressed in terms of the differential baseline vector $\delta\bar{B}$ as

$$B(r,a) = \frac{4\pi}{\lambda}\hat{n}\cdot\delta\bar{B} \tag{23}$$

Since two (upper antenna and lower antenna) images are co-registered in the along track direction, the differential baseline vector can be written as

$$\delta\bar{B} = \delta B_c\hat{c} + \delta B_h\hat{h} \tag{24}$$

This baseline calibration is actually the calibration of two vectors from the motion measurement system to both antennas. The look vector $\hat{n}$ is in the direction of the Doppler centroid used for the data processing and it is given by

$$\begin{aligned}\hat{n} &= (-\sin\theta\sin\theta_y - \cos\theta\cos\theta_y\sin\theta_p)\hat{s}\\ &+(-\sin\theta\cos\theta_y + \cos\theta\sin\theta_y\sin\theta_p)\hat{c}\\ &+\cos\theta\cos\theta_p\hat{h}\end{aligned} \tag{25}$$

where θ_p and θ_y are the pitch and the yaw angle, respectively.

It is well known that the co-polarized phase difference can be used for classification since it comes from the scattering center displacement; however, for the forest area, the co-polarized phase appears to be random since the phase center displacement may be larger than the wavelength. This problem can be solved if polarimetric interferometry is implemented and the interferometric phase difference is above the phase noise level. That is, since the interferometric ambiguity height is much larger than the tree height, the interferometric technique unwraps the polarimetric phase difference. The polarization dependent interferometric correlation also can be used for land classification applications.

5. CONCLUSIONS

In this paper, we presented various representations of the scattering mechanism in terms of SAR polarimetry, SAR interferometry, and SAR polarimetric interferometry. In order to use SAR data for science applications, desired geophysical parameters must be measurable when SAR data are properly enhanced. The relationship between SAR data and geophysical parameters can be obtained by both theoretical and empirical approaches. The techniques shown in this paper can be used to derive useful geophysical parameters from SAR data. In order to achieve this goal, SAR data must be calibrated. Especially, the polarimetric interferometry calibration requirement is difficult accomplish; therefore, a new technique must be derived. In this paper, we proposed a technique for the polarimetric interferometry calibration. We expect that SAR polarimetric interferometry will provide detailed scattering mechanism of each pixel that can be used for various science applications such as the tree height estimation and land classification.

REFERENCES

[1] F. M. Handerson and A. J. Lewis ed., *Principles & Applications of Imaging Radar*, Manual of Remote Sensing, Third Edition, Volume 2, John Wiley & Sons, New York, 1998.

[2] J. J. van Zyl, H. A. Zebker, and C. Elachi, " Imaging Radar Polarization Signatures: Theory and Observation," *Radio Scienece*, Vol. 22, 529-543, 1987.

[3] L. C. Graham, "Synthetic Interferometer Radar for Topographic Mapping, *Proceedings of IEEE*, Vol. 62, 763-768, 1974.

[4] S. R. Cloude and K. P. Papathanassiou, "Polarimetric SAR Interferometry," *IEEE Trans. Geosci. Remote Sens.*, GE-36, 1551-1565, 1998.

[5] J. J. van Zyl, H. A. Zebker, and C. Elachi, Polarimetric SAR Applications, *Radar Polarimetry for Geoscience Applications (F. T. Ulaby and C. Elachi ed.)*, Artech House, Norwood, MA, 315-360, 1990.

[6] E. Rodriguez, T. R. Michel, and D. J. Harding, "Interferometric measurement of canopy height characteristics for coniferous forests, submitted for publication.

[7] R. N. Treuhaft and P. R. Siqueira, "The vertical structure of vegetated land surfaces from interferometric and polarimetric radar," submitted to Radio Science.

[8] Y. Kim, J. J. van Zyl, and A. Chu, "Preliminary Results of Single Pass Polarimetric SAR Interferometry," IGARSS '99.

Yunjin Kim *received the Ph. D. degree from the University of Pennsylvania in 1987. From 1987 to 1989, he was with the Department of Electrical Engineering, New Jersey Institute of Technology, as an Assistant Professor. Since 1989, he has been with the Jet Propulsion Laboratory. Currently, Dr. Kim is the radar science and engineering section manager at Jet propulsion Laboratory. He is also an Associate Editor of Radio Science. His current research area includes SAR polarimetry and interferometry, SAR data calibration and processing, SAR data applications, radar system engineering, electromagnetic scattering, and advanced radar technology development. He received the NASA Exceptional Service Medal in 1995.*

Jakob J van Zyl *was born in Outjo, Namibia in 1957. He received the Hons. B. Eng. degree cum laude in electronics engineering from the University of Stellenbosch, Stellenbosch, South Africa, in 1979, and also received the Siemens prize for best achievement in the graduating class from the electrical engineering department. He received the M.S. and Ph.D. degrees in electrical engineering from the California Institute of Technology, Pasadena, in 1983 and 1986, respectively. Dr. van Zyl received the 1997 Fred Nathanson Memorial Radar Award to the Young Engineer of the Year from the IEEE Aerospace and Electronics Systems Society.*

In 1984 he was the recipient of a Schlumberger Foundation fellowship. He was teaching assistant for a course on "Physics of Remote Sensing" at the California Institute of Technology from 1983 to 1986. He joined the Jet Propulsion Laboratory in Pasadena, California in 1986, where he worked as a research scientist (1986-1990), the supervisor of the Airborne SAR Group (1990-1995), and the Manager of the Radar Science and Engineering Section (1995-1998). At present he is the Deputy Program Manager of the Earth Science Flight Projects Office. Dr. van Zyl teaches "Remote Sensing Systems from Space" during the fall semester at the University of Southern California as an adjunct Faculty Member in the Aerospace Engineering Department, as well as part of a Short Course "Synthetic Aperture Radar: Understanding the Imagery" at UCLA. He is a five-year member of the Institute for Electromagnetics Modeling and Applications of The Electromagnetics Academy. Dr. van Zyl has contributed to ten books and published more than forty papers in peer reviewed journals. His current research interests include studying theoretical electromagnetic problems related to polarimetric scattering, remote sensing, and the analysis of interferometric and polarimetric SAR data.

ACKNOWLEDGMENT

The research described in this paper was carried out by the Jet Propulsion Laboratory, California Institute of Technology, under a contract with the National Aeronautics and Space Administration.